Optics and Lasers in Engineering 98 (2017) 83–88

Contents lists available at ScienceDirect

Optics and Lasers in Engineering

journal homepage: www.elsevier.com/locate/optlaseng

Image hiding scheme based on time-averaged elliptic oscillations

Loreta Saunoriene[a], Sandra Aleksiene[a], Rimas Maskeliunas[b], Minvydas Ragulskis[a,*]

[a] Research Group for Mathematical and Numerical Analysis of Dynamical Systems, Kaunas University of Technology, Studentu 50, Kaunas LT-51368, Lithuania
[b] Department of Printing Machines, Vilnius Gediminas Technical University, J. Basanaviciaus 28, Vilnius LT-03224, Lithuania

ARTICLE INFO

Keywords:
Image hiding
Elliptic oscillations
Time-averaged moiré
Cover image

ABSTRACT

Image hiding technique based on time-averaged elliptic oscillations is proposed in this paper. The scheme is based on a single cover image representing a cross-moiré grating. The secret image is embedded into the background moiré grating by using a specially developed random scrambling algorithm. The secret is leaked in a form of a pattern of time-averaged moiré fringes when the cover image is elliptically oscillated. Also, the secret is leaked only if the parameters of elliptic oscillations are set to predefined values. Computational experiments are used to validate the proposed technique and to demonstrate the efficiency of its implementation.

1. Introduction

A dichotomous secret image hiding scheme based on time-averaged techniques used for the registration of the oscillating encoded cover image is a well-known approach in geometric moiré optics [1,2]. Conditionally, such an image hiding scheme can be entitled as dynamic visual cryptography (DVC) [2,3]. Classical visual cryptography (VC) is a cryptographic technique which allows visual information (pictures or text) to be encrypted in such a way that the decryption can be performed solely by the human visual system [4]. The decryption of the secret in a VC scheme does not require a computer. However, any VC scheme is a visual secret sharing scheme – the secret image is broken up into a number of shares so that only someone with all shares could decrypt the image [5,6]. Each share is usually printed on a separate transparency, and decryption is performed by simply overlaying the shares.

The DVC scheme is similar to the VC scheme in the sense that a computer is not required for performing the decryption of the secret. The secret image is embedded into one cover image, which must be oscillated in order to leak the secret [1,2]. Time-averaging optical techniques are used to register the oscillating cover image (the exposure time must be much longer than a single period of periodic oscillations) [1]. Thus, the DVC scheme does not employ image sharing – a single cover image is used instead.

Any image hiding scheme – VC or DVC has its own drawbacks. Complex means are used to eliminate the probability of cheating in VC schemes [7–9]. Special chaotic scrambling algorithms are required to embed the secret into the single cover image in DVC schemes [1].

The security of DVC schemes can be improved by generating such stochastic moiré gratings that the secret image is leaked from only when the cover image is oscillated according to a periodic (but non-harmonic) time function – but the secret is not leaked at any amplitude or any direction of uni-directional harmonic oscillations [2]. Chaotic time functions [3], special moiré grating optimization techniques [10], deformable moiré gratings [11] can be used to further increase the security of DVC schemes.

All up-mentioned DVC schemes are based on uni-directional oscillations of the cover image. However, it is well known that generation of uni-directional oscillations can be a challenging problem even for harmonic oscillations – especially when the considered engineering structures comprise many degrees of freedom or are nonlinear [12]. A simple uni-directional forcing of such structures can result into complex (even chaotic) trajectories of motion [13]. In this paper we consider the one of the simplest cases of such effects – elliptical oscillations.

On the other hand, the employment of elliptical oscillations opens a completely new approach for the generation of the cover image. Uni-directional oscillations enable to exploit a simple and straightforward strategy for the construction of the cover image – every column (row) of such an image can be interpreted as an isolated one-dimensional array of pixels. In principal, DVC schemes based on uni-directional oscillations can be considered as one-dimensional problems (except the chaotic scrambling algorithm which is used to hide the secret image – but does not affect the structure of any of the one-dimensional gratings) [1]. Such DVC schemes based on uni-directional oscillations are highly sensitive to changes of the direction of oscillation – the secret image becomes non-interpretable if the angle between the orientation

* Corresponding author.
E-mail address: minvydas.ragulskis@ktu.lt (M. Ragulskis).

http://dx.doi.org/10.1016/j.optlaseng.2017.06.009
Received 13 January 2017; Received in revised form 3 April 2017; Accepted 10 June 2017
0143-8166/

of one-dimensional moiré gratings and the direction of one-directional oscillations becomes higher than 5 degrees [1].

It is clear that the construction of the cover image for a DVC scheme based on elliptic oscillations must be based on a completely different approach – this becomes a full two-dimensional problem. The main objective of this paper is to develop such a DVC scheme based on elliptical oscillations.

2. Preliminaries

One-dimensional moiré grating can be interpreted as a harmonic variation of grayscale color [12]:

$$F(x) = \frac{1}{2} + \frac{1}{2}\cos\left(\frac{2\pi}{\lambda}x\right), \tag{1}$$

where x is the longitudinal coordinate, λ is a pitch of moiré grating in the state of equilibrium. Numerical value 0 of function $F(x)$ corresponds to black color, 1 – to white color, values from the interval (0, 1) correspond to an appropriate grayscale level.

Let us consider that moiré grating in Eq. (1) is harmonically oscillated around the state of equilibrium according to the deflection function:

$$u(t) = a\sin(\omega t + \varphi), \tag{2}$$

where a is the amplitude of harmonic oscillations; ω is the cyclic frequency and φ is the phase. One-dimensional time averaged image reads [1,12]:

$$\lim_{T\to\infty}\frac{1}{T}\int_0^T\left(\frac{1}{2} + \frac{1}{2}\cos\left(\frac{2\pi}{\lambda}(x - a\sin(\omega t + \varphi))\right)\right)dt = \frac{1}{2} + \frac{1}{2}\cos\left(\frac{2\pi}{\lambda}x\right)J_0\left(\frac{2\pi}{\lambda}a\right) \tag{3}$$

where T is the exposure time; J_0 is the zero order Bessel function of the first kind.

Note that the resulting time averaged image does not depend on ω. However, since the exposure time cannot be infinite in any physical experiment, the cyclic frequency becomes an important factor. A large number of periods of oscillation must fit into a finite exposure time in order to minimize optical effects introduced by the fractional part of the last period (unless the exposure time is exactly fitted to the period of oscillation) [1]. The situation is even more complex from the biomedical point of view [11]. A naked eye follows the slow oscillation of the cover image, and human visual system is not able to interpret the time averaged image then. The holistic human visual system (including eyes, nerves, visual cortex) can interpret the time averaged image only when the cyclic frequency is high enough (usually over 30 Hz) and eye balls cannot longer track the cover image [11].

Time averaged image becomes grey when the amplitude of harmonic oscillations is equal to:

$$a = \frac{\lambda}{2\pi}r_i, \tag{4}$$

where r_i is the ith root of J_0. This optical effect is illustrated in Fig. 1. Stationary one-dimensional moiré grating is shown at the left side of Fig. 1(a) (where the amplitude $a = 0$). Note that the moiré grating is constructed only in a finite interval $6 \le x \le 26$ and the white background is assumed elsewhere. Time averaged image of an oscillating one-dimensional moiré grating (note that the time averaged image does not depend on the frequency of oscillations) is visualized as a column of pixels at every discrete value of the amplitude a (Fig. 1(a)). The graph of $J_0\left(\frac{2\pi}{\lambda}a\right)$ is shown in Fig. 1(b); dashed vertical lines mark roots of J_0. It can be clearly seen that the centerlines of time-averaged moiré fringes coincide with the roots of J_0 (Fig. 1(a) and (b)).

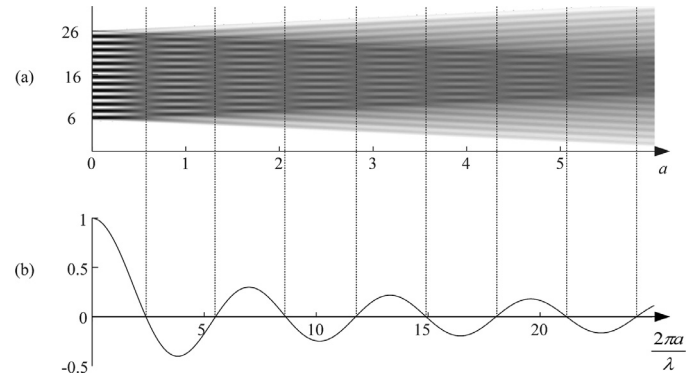

Fig. 1. Pattern of time averaged fringes at $\lambda = 1.5$: (a) an array of grayscale one-dimensional time averaged images at monotonously increasing amplitude of transverse harmonic oscillations; (b) zero order Bessel function of the first kind $J_0(2\pi a/\lambda)$; dashed lines interconnect the centers of time averaged fringes and roots of the Bessel function.

3. Two-dimensional moiré gratings

3.1. Simple moiré gratings in two dimensions

An array of parallel black and white lines on a flat surface can be described by the following formula [12]:

$$F(x, y) = \frac{1}{2} + \frac{1}{2}\cos\left(\frac{2\pi}{\lambda}x\right), \tag{5}$$

where x is the longitudinal coordinate; λ is a pitch along the moiré grating; y-axis coincides with the direction of the constitutive grating lines. In analogy to the one-dimensional grating, we assume that the surface performs harmonic oscillations as a non-deformable body. Unidirectional oscillations of the two-dimensional non-deformable surface along the x-axis yield:

$$\lim_{T\to\infty}\frac{1}{T}\int_0^T F(x - a\sin t, y)dt = \lim_{T\to\infty}\frac{1}{T}\int_0^T\left(\frac{1}{2} + \frac{1}{2}\cos\left(\frac{2\pi}{\lambda}(x - a\sin t)\right)\right)dt = \frac{1}{2} + \frac{1}{2}\cos\left(\frac{2\pi}{\lambda}x\right)J_0\left(\frac{2\pi}{\lambda}a\right). \tag{6}$$

Time averaged image becomes a uniformly gray surface at $a = \frac{\lambda}{2\pi}r_i$. On the other hand, oscillations along the y-axis do not alter the static image:

$$\lim_{T\to\infty}\frac{1}{T}\int_0^T F(x, y - a\sin t)dt = \lim_{T\to\infty}\frac{1}{T}\int_0^T\left(\frac{1}{2} + \frac{1}{2}\cos\left(\frac{2\pi}{\lambda}x\right)\right)dt = \frac{1}{2} + \frac{1}{2}\cos\left(\frac{2\pi}{\lambda}x\right). \tag{7}$$

This is a well-known effect in experimental mechanics that deformations along constitutive lines of a grating do not change the optical image of the surface [12,14].

3.2. Two-dimensional cross-gratings; unidirectional oscillations

A static two-dimensional cross-grating is described by:

$$F_2(x, y) = \frac{1}{2} + \frac{1}{2}\cos\left(\frac{2\pi}{\lambda}x\right)\cos\left(\frac{2\pi}{\mu}y\right), \tag{8}$$

where λ – is the pitch of the grating in the horizontal direction; μ is the pitch in the vertical direction. An example of a two-dimensional moiré cross-grating with $\lambda = 0.75$ and $\mu = 0.5$ is illustrated in Fig. 2(a).

If a cross-grating in Eq. (8) is oscillated along the x- and y-axis, the resulting time-averaged image reads:

Fig. 2. Unidirectional oscillations of two-dimensional cross-grating: (a) the static image at $\lambda = 0.75$, $\mu = 0.5$; (b) time averaged image in case of vertical unidirectional oscillations at $b = 0.4393$; (c) time averaged image in case of horizontal unidirectional oscillations at $a = 0.2871$.

$$\lim_{T\to\infty}\frac{1}{T}\int_0^T F_2(x - a\sin t, y)dt = \frac{1}{2} + \frac{1}{2}\cos\left(\frac{2\pi}{\lambda}x\right)\cos\left(\frac{2\pi}{\mu}y\right)J_0\left(\frac{2\pi}{\lambda}a\right), \tag{9}$$

$$\lim_{T\to\infty}\frac{1}{T}\int_0^T F_2(x, y - b\sin t)dt = \frac{1}{2} + \frac{1}{2}\cos\left(\frac{2\pi}{\lambda}x\right)\cos\left(\frac{2\pi}{\mu}y\right)J_0\left(\frac{2\pi}{\mu}b\right), \tag{10}$$

where a and b are amplitudes of harmonic oscillations along the x-axis and y-axis respectively.

In other words, the cross-grating is blurred into a uniformly gray image if only the amplitude of harmonic oscillations (along the x-axis or along the y-axis) is such that the zero order Bessel function of the first kind turns to 0. These effects are illustrated in Fig. 2(b) and (c).

If unidirectional oscillations are inclined at angle $\varphi = \arctan\left(\frac{b}{a}\right)$ in respect to the x-axis, then elementary trigonometric manipulation yields the following expression of the time-averaged image:

$$\begin{aligned}&\lim_{T\to\infty}\frac{1}{T}\int_0^T F_2(x - a\sin t, y - b\sin t)dt\\ &= \frac{1}{2} + \frac{1}{4}\cos\left(\frac{2\pi}{\lambda}x\right)\cos\left(\frac{2\pi}{\mu}y\right)\left(J_0\left(\frac{2\pi}{\lambda}a + \frac{2\pi}{\mu}b\right) + J_0\left(\frac{2\pi}{\lambda}a - \frac{2\pi}{\mu}b\right)\right)\\ &+\frac{1}{4}\sin\left(\frac{2\pi}{\lambda}x\right)\sin\left(\frac{2\pi}{\mu}y\right)\left(J_0\left(\frac{2\pi}{\lambda}a - \frac{2\pi}{\mu}b\right) - J_0\left(\frac{2\pi}{\lambda}a + \frac{2\pi}{\mu}b\right)\right).\end{aligned} \tag{11}$$

Now, if the parameters of unidirectional oscillations are linked by the equality $\frac{a}{\lambda} = \frac{b}{\mu}$, then Eq. (11) yields:

$$\begin{aligned}&\lim_{T\to\infty}\frac{1}{T}\int_0^T F_2\left(x - a\sin t, y - a\frac{\mu}{\lambda}\sin t\right)dt\\ &= \frac{1}{2} + \frac{1}{4}\cos\left(\frac{2\pi}{\lambda}x\right)\cos\left(\frac{2\pi}{\mu}y\right)\left(J_0\left(\frac{4\pi}{\lambda}a\right) + 1\right)\\ &+\frac{1}{4}\sin\left(\frac{2\pi}{\lambda}x\right)\sin\left(\frac{2\pi}{\mu}y\right)\left(1 - J_0\left(\frac{4\pi}{\lambda}a\right)\right)\\ &= \frac{1}{2} + \frac{1}{4}\left(\cos\left(\frac{2\pi}{\lambda}x - \frac{2\pi}{\mu}y\right) + \cos\left(\frac{2\pi}{\lambda}x + \frac{2\pi}{\mu}y\right)J_0\left(\frac{4\pi}{\lambda}a\right)\right).\end{aligned} \tag{12}$$

Appropriate selection of parameters a and b ($a = \frac{\lambda}{4\pi}r_i$ and $b = \frac{\mu}{4\pi}r_i$, $i = 1, 2, \ldots,$) yields:

$$\begin{aligned}&\lim_{T\to\infty}\frac{1}{T}\int_0^T F_2\left(x - \frac{\lambda}{4\pi}r_i\sin t, y - \frac{\mu}{4\pi}r_i\sin t\right)dt\\ &= \frac{1}{2} + \frac{1}{4}\cos\left(\frac{2\pi}{\lambda}x - \frac{2\pi}{\mu}y\right).\end{aligned} \tag{13}$$

In other words, the cross-grating is transformed into an array of inclined lines in the time-averaged image. This interesting optical effect is illustrated in Fig. 3.

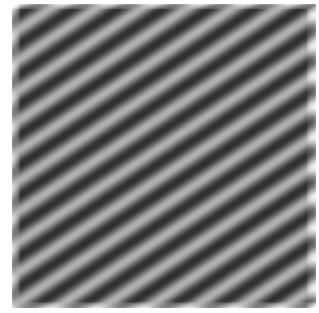

Fig. 3. Unidirectional oscillations of the non-deformable grating in Fig. 2(a) results into an array of inclined lines at $a = 0.1435$, $b = 0.0957$, $\varphi = \frac{\pi}{4}$.

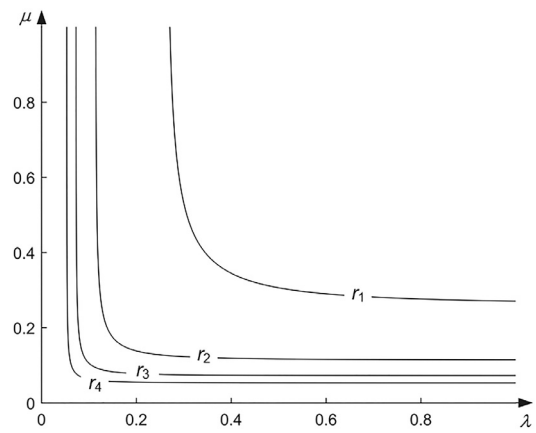

Fig. 4. The relationship between grating parameters λ and μ at $A = 0.1$; different curves correspond to the different values of r_i, $i = 1, 2, 3, 4$.

3.3. Two-dimensional cross-gratings. Elliptic oscillations

Let us assume that the deflection of a two-dimensional cross-grating around the state of equilibrium is elliptic; the radiuses of the ellipse are a and b. Then elementary trigonometric manipulation yields:

$$\begin{aligned}&\lim_{T\to\infty}\frac{1}{T}\int_0^T F_2(x - a\sin t, y - b\cos t)dt\\ &= \frac{1}{2} + \frac{1}{2}\cos\left(\frac{2\pi}{\lambda}x\right)\cos\left(\frac{2\pi}{\mu}y\right)J_0(M).\end{aligned} \tag{14}$$

where

$$M = \sqrt{\left(\frac{2\pi}{\lambda}a\right)^2 + \left(\frac{2\pi}{\mu}b\right)^2}; \quad \varphi = \arctan\left(\frac{b\lambda}{a\mu}\right). \tag{15}$$

Thus, the time-averaged image becomes uniformly gray when the following equality holds true:

$$\left(\frac{2\pi}{\lambda}a\right)^2 + \left(\frac{2\pi}{\mu}b\right)^2 = (r_i)^2; \quad i = 1, 2, \ldots, . \tag{16}$$

If $a = b = A$, then Eq. (16) reduces to an explicit relationship between λ and μ:

$$\lambda = \frac{1}{\sqrt{\left(\frac{r_i}{2\pi A}\right)^2 - \frac{1}{\mu^2}}}; \quad \mu > \frac{2\pi A}{r_i}; \quad i = 1, 2, \ldots, . \tag{17}$$

Graphical representation of Eq. (17) is shown in Fig. 4.

4. Hiding secret in two-dimensional cross-gratings

Let us consider the secret image represented as a black circle illustrated in Fig. 5(a). Let us construct the background image as a two-dimensional cross-grating with parameters $\lambda = 1.7$ and $\mu = 1.7$

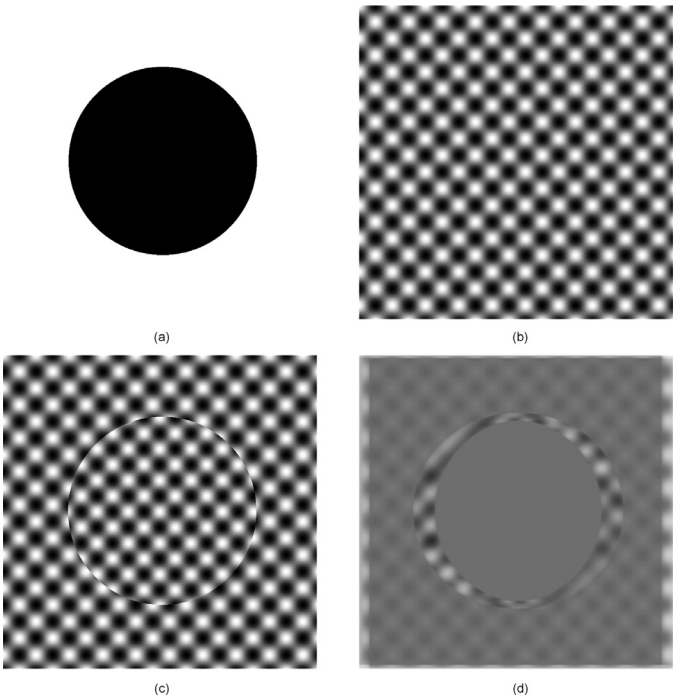

Fig. 5. A straightforward embedding of a geometrical shape into the background image does not result into an acceptable cover image: (a) the secret image (the black disk); (b) static background moiré grating at $\lambda = 1.7$, $\mu = 1.7$; (c) a straightforward embedding produces a clear boundary line between the background and the secret ($\lambda = 1.6$, $\mu = 1.6$ are used in the area of the secret image); (d) computational decryption using elliptic oscillations at $a = 0.5788$, $b = 0.2$.

(Fig. 5(b)). The secret image (the circle) is also represented as a two-dimensional cross-grating but with different pitches ($\lambda = 1.6$; $\mu = 1.6$) (Fig. 5(c)). The boundary line between the background and the secret image is clearly visible in Fig. 5(c) – thus such an approach cannot be considered as an image hiding technique. Nonetheless, an appropriate selection of the parameters of the elliptic motion ($a = 0.5788$; $b = 0.2$) produces a uniformly gray zone in the area occupied by the secret image in the time-averaged image – while the background represents a non-fully developed time-averaged moiré fringe (Fig. 5(d)). Note that the border line between the background and the secret produces a band of non-developed fringes due to the elliptic motion of the cover image (Fig. 5(d)).

It is clear that more sophisticated image hiding techniques are required than illustrated in Fig. 5. Unfortunately, stochastic moiré gratings cannot be employed for elliptic oscillations – thus any initial phase scrambling algorithms would not help to hide the secret image. One of the possible solutions is to minimize the differences between pitches in the background and the secret image – yet the differences should be large enough to enable optical discrimination between the secret and the background in the time-averaged image [1].

Thus the main idea of the encoding secret information in two dimensional moiré grid (Eq. (8)) is based on increasing the values of λ and μ by small quantities λ^* and μ^*:

$$F_2(x, y) = \frac{1}{2} + \frac{1}{2}\cos\left(\frac{2\pi x}{\lambda + \lambda^*}\right)\cos\left(\frac{2\pi y}{\mu + \mu^*}\right), \tag{18}$$

where λ^* and μ^* ($\lambda^* \ll \lambda$ and $\mu^* \ll \mu$) are small positive numbers within the area occupied by the image (and are equal to zero in the background).

It can be noted, that the influence of terms λ^* and μ^* in Eq. (18) increases when the coordinates x and y increase (as illustrated in Fig. 6). Solid line in Fig. 6(c) illustrates this fact – the difference between values of $\frac{2\pi x}{\lambda+\lambda^*}$ and $\frac{2\pi x}{\lambda}$ increases when x increases. Analogously, the difference between values $\frac{2\pi y}{\mu+\mu^*}$ and $\frac{2\pi y}{\mu}$ increases when y increases. Therefore, we need to find such functions $\lambda^* = l(x)$ and $\mu^* = m(y)$, which ensure the constant variation of values $\frac{2\pi x}{\lambda+\lambda^*}$ and $\frac{2\pi y}{\mu+\mu^*}$ for any x and y respectively:

$$\begin{aligned} &\frac{2\pi x}{\lambda} - \frac{2\pi x}{\lambda + l(x)} = \delta, \quad 0 \le x \le x_{max}; \\ &\frac{2\pi y}{\mu} - \frac{2\pi y}{\mu + m(y)} = \delta, \quad 0 \le y \le y_{max}; \end{aligned} \tag{19}$$

where x_{max} and y_{max} define the coordinate system of the rectangular cover image; δ is the threshold value ensuring the minimal difference of a two-dimensional moiré pitch resulting into an interpretable difference image in time-averaged mode. We assume that δ is equal to 0 in the background and is equal to predefined number in the area occupied by the secret image. Eq. (19) lead to the following expressions of $l(x)$ and $m(y)$:

$$\begin{aligned} l(x) &= \frac{\lambda\delta}{2\pi x - \delta}; \\ m(y) &= \frac{\mu\delta}{2\pi y - \delta}. \end{aligned} \tag{20}$$

The dotted line in Fig. 6(b) and (c) shows the variation of $\frac{2\pi}{\lambda+l(x)}$ and $\frac{2\pi x}{\lambda+l(x)}$ respectively. In this example δ is obtained from the equality $l(\frac{x_{max}}{2}) = \lambda^*$.

As mentioned previously, all image hiding schemes based on dynamic visual cryptography are not cryptographically secure. The main requirement is that the secret image should not be leaked from the stationary cover image by a naked eye. Therefore, the optical security of the proposed image hiding scheme can be improved by adding the random noise to the value δ. Fig. 6(d) shows the variation of $\frac{2\pi x}{\lambda+l(x)}$ with the random scrambling of δ.

Fig. 7 illustrates the implementation of the image hiding technique based on elliptic oscillations. The secret image is assumed to comprise numbers “1 2 3” and “A B C”. The width of the alphanumerical symbols is selected to be equal to the half of the pitch of the cross-grating in the background. That corresponds to the minimal size of an embedded square-shaped object into a stochastic moiré grating for unidirectional decoding [11]. Fig. 7(a) shows the values of δ used for the encoding of the secret. The cover image is constructed as a deformed two-dimensional cross-grating (Fig. 7(b)). We consider the image is 12x12 rectangle, with pitches of two-dimensional grating $\lambda = 0.8$ and $\mu = 0.68$. It is clear that the secret information cannot be leaked by a naked eye from the cover image (Fig. 7(b)). The decrypted image is obtained by oscillating the cover image elliptically with amplitudes equal to $a = 0.25$ and $b = 0.15$. As it was discussed in the Section 3.3, parameters λ, μ, a and b must correspond to the relationship Eq. (16) in order to produce time-averaged moiré fringes. Original and contrast enhanced time averaged images are presented in Fig. 7(c) and (d). Note that the size of the decrypted symbols in the time averaged image (Fig. 7(d)) is larger compared to the size of the encoded symbols (Fig. 7(a)). This is due to elliptic oscillations – the boundaries of the symbols are blurred. The larger are the radiuses of the ellipse, the wider are the blurred boundaries. Fig. 8 illustrates the failure to leak the secret image at improper amplitudes of elliptic oscillations. Not fully developed pattern of time averaged moiré fringes is shown in Fig. 8(a) when the parameters of elliptic oscillations are set to $a = 0.26$, $b = 0.16$. The time averaged image is completely not interpretable at $a = 0.29$, $b = 0.19$ (Fig. 8(c)).

It can be observed that the information capacity of the proposed scheme (the quantity of secret information that can be embedded into the cover image) is not worse than the capacity of the scheme described in [11].

5. Concluding remarks

The image hiding technique based on elliptic oscillations is proposed in this paper. The cover image is produced as a deformed two-dimensional cross-moiré grating. The encrypted secret image appears in

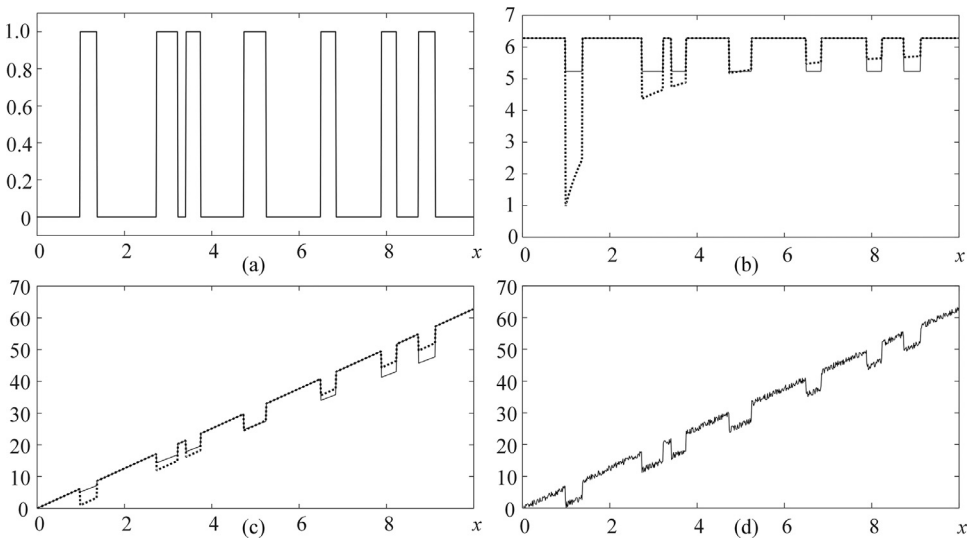

Fig. 6. One-dimensional illustration of the random scrambling algorithm of δ. (a) a schematic illustration of the secret information (value 1 corresponds to the secret information; 0 corresponds to the background); (b) variation of $\frac{2\pi}{\lambda+\lambda^*}$ (the solid line) and $\frac{2\pi}{\lambda+l(x)}$ (the dotted line); (c) variation of $\frac{2\pi x}{\lambda+\lambda^*}$ (the solid line) and $\frac{2\pi x}{\lambda+l(x)}$ (the dotted line); (d) variation of $\frac{2\pi x}{\lambda+l(x)}$ with the randomly scrambled value of δ.

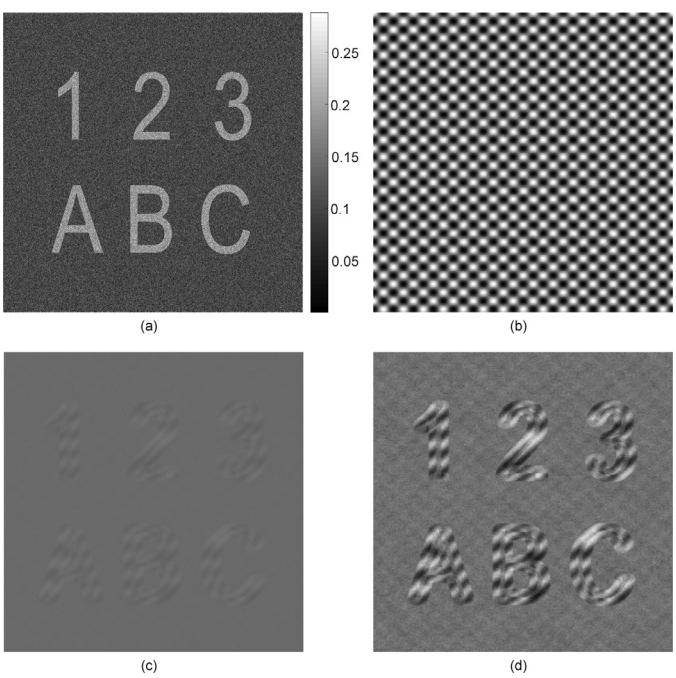

Fig. 7. Image hiding scheme based on elliptic oscillations: (a) values of $\delta(x, y)$ corresponding to the stationary secret image; (b) the stationary cover image at $\lambda = 0.8$, $\mu = 0.68$ (a naked eye cannot interpret the embedded secret); (c) the time-averaged image of the cover image performing elliptic oscillations at $a = 0.25$, $b = 0.15$; (d) the contrast enhancement of the time-averaged image produces clear contours of the secret image.

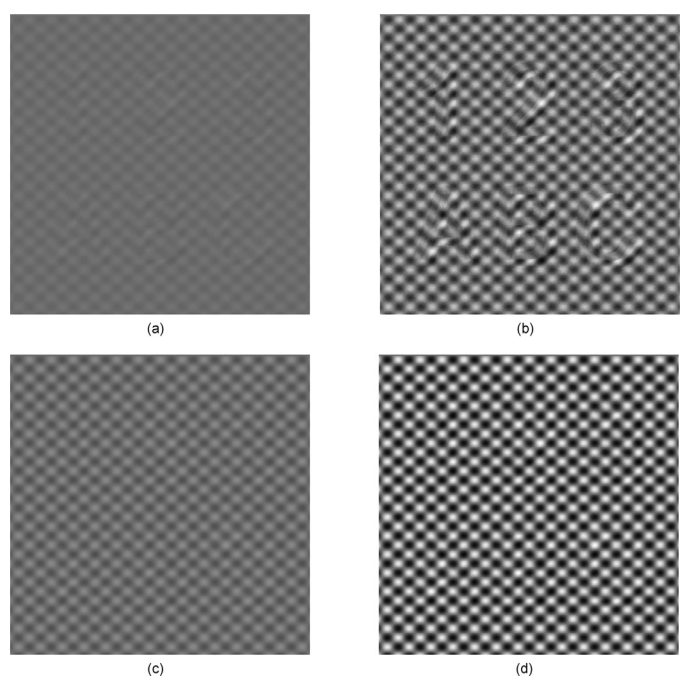

Fig. 8. Improper amplitudes of elliptic oscillations does not leak the secret information: (a) not fully developed pattern of time averaged moire fringes at $a = 0.26$, $b = 0.16$; (b) the contrast enhancement of the time-averaged image (at $a = 0.26$, $b = 0.16$) yields almost non-interpretable contours of the secret image; (c) the time-averaged image of the cover image does not leak the secret at $a = 0.29$, $b = 0.19$; (d) the contrast enhancement of the time-averaged image (at $a = 0.29$, $b = 0.19$) does not produce any contours of the secret image.

a form of time-averaged moiré fringes when the cover image is oscillated according to an elliptic law of motion.

The proposed image hiding technique does possess the basic properties of dynamic visual cryptography scheme. Special computational algorithms are required to embed the secret image into the cover image – but a computational device is not required to decrypt the secret. The secret is leaked in the form of a pattern of time-averaged moiré fringes when the cover image is oscillated according to an elliptical law of motion. This is an image hiding scheme employing a single cover image and does not require an optical superposition of any shares. In other words, the proposed scheme does not use any image sharing or pixel expansion algorithms to embed the secret.

The principal difference between image hiding schemes based on uni-directional oscillations and elliptic oscillation is in the secret embedding algorithm. One-dimensional columns (rows) of pixels can be randomly scrambled in image hiding schemes based on uni-directional oscillations. Such random scrambling techniques are not applicable for image hiding schemes based on elliptic oscillations because the one-dimensional structure of moiré gratings is damaged in the time-averaged

mode. New secret image hiding technique are developed to overcome these difficulties in order to ensure an effective optical decryption of the secret.

Such image hiding techniques based on elliptic oscillations do have a definite potential for a variety of practical applications. As mentioned previously, uni-directional excitation of complex structures does not necessarily result into a uni-directional oscillation of the excited structure. Therefore, the proposed technique opens new possibilities for optical control of vibration generation equipment. Experimental implementation of the proposed optical technique is a definite objective of future research.

Acknowledgments

Financial support from the Research Council of Lithuania under Project no. MIP-078/2015 is acknowledgd.

References

[1] Ragulskis M, Aleksa A. Image hiding based on time-averaging moiré. Opt Commun 2009;282:2752–9.
[2] Ragulskis M, Aleksa A, Navickas Z. Image hiding based on time-averaged fringes produced by non-harmonic oscillations. J Opt A 2009;11:125411 (11pp).
[3] Petrauskiene V, Aleksa A, Fedaravicius A, Ragulskis M. Dynamic visual cryptography for optical control of vibration generation equipment. Opt Lasers Eng 2012;50(6):869–76.
[4] Naor M, Shamir R. Visual cryptography. Lect Notes Comput Sci 1994;950:1–12.
[5] Verma J, Khemchandani V. A visual cryptographic technique to secure image shares. Int J Eng Res Appl (IJERA) 2012;2(1). 1121
[6] Feng JB, Wu HC, Tsa CS, Chang YF, Chu YP. Visual secret sharing for multiple secrets. Pattern Recognit 2008;41:3572–81.
[7] Chen YC, Tsai DS, Horng G. A new authentication based cheating prevention scheme in Naor–Shamir's visual cryptography. J Visual Commun Image Represent 2012;23(8):1225–33.
[8] Horng G, Chen T, Tsai DS. Cheating in visual cryptography. Des Codes Cryptogr 2006;38(2):219–36.
[9] Hu CM, Tzeng WG. Cheating prevention in visual cryptography. IEEE Trans Image Process 2007;16(1):36–45.
[10] Sakyte E, Palivonaite R, Aleksa A, Ragulskis M. Image hiding based on near-optimal moiré gratings. Opt Commun 2011;284:3954–64.
[11] Palivonaite R, Aleksa A, Paunksnis A, Gelzinis A, Ragulskis M. Image hiding in time-averaged deformable moiré gratings. J Opt 2014;16:025401 (8pp).
[12] Kobayashi AS. Handbook on experimental mechanics. 2nd. Bethel, CT: SEM; 2000.
[13] Hilborn R. Chaos and nonlinear dynamics: an introduction for scientists and engineers. Oxford: Oxford University Press; 1994.
[14] Patorski K, Kujawinska M. Handbook on the moiré fringe technique. Amsterdam: Elsevier; 1993.